Indian Journal of Pure & Applied Physics
Vol. 52, July 2014, pp. 450-456

Spatial emission characteristics from electron oscillation driven by a circularly polarized few-cycle laser pulse

Youwei Tian[a,*], Yang Yu[b], Jiasong Zhu [a], Lei Zhang[a], Liangling Bian[a], Mengsi Jin[a], Qiuyuan Zhang[a], Haiyang Lu[c] & Vinod Senecha[d]

[a]College of Science, Nanjing University of Posts and Telecommunications, Nanjing 210003, People's Republic of China

[b]School of Mechinery and Automobile Engineering, Hefei University of Technology. Hefei 230009, People's Republic of China

[c]State Key Laboratory of High Field Laser Physics, Shanghai Institute of Optics and Fine Mechanics, Chinese Academy of Sciences, Shanghai 201800, People's Republic of China

[d]Raja Ramanna Centre for Advanced Technology, Indore 452 013, India

*E-mail: tianyw@njupt.edu.cn

Received 17 September 2013; revised 13 December 2013; accepted 15 April 2014

Full spatial emission characteristics of radiation generated from electron oscillations driven by a circularly polarized few-cycle laser pulse of different intensity have been investigated theoretically and numerically using a single electron model. The effect of laser pulse intensity and the initial phase on the process of full spatial characteristics of the radiation is apparent for few-cycle laser pulse. The characteristics can be used to measure the intensity and the initial phase of a circularly polarized few-cycle laser pulse in experiments.

Keywords: Full spatial distribution, Electron oscillation, Circularly polarized few-cycle laser pulses

1 Introduction

With the advent of ultrashort pulse high-power lasers, it has now become possible via strong focusing to extend the irradiance to the levels of 10^{19}W/cm^2 and with petawatt level lasers intensities much higher than this can be achieved[1]. In the intense laser field, the electron dynamics becomes highly relativistic and then many nonlinear effects start playing a role in the nonlinear scattering process[2-18]. Further, the radiation generated by relativistic electrons is also frequency up-shifted by the relativistic Doppler effect[4]. In addition, He *et al*[5]. studied the effect of the electron initial conditions, such as the electron initial position or initial time injecting on the laser field, on electron dynamics and radiation. All the above works treat the laser field as a plane wave approximately. Lee *et al*[6]. extended the above analytic investigations of nonlinear scattering to case of the multi-cycle laser pulse case. They investigated the temporal and spectral characteristics of nonlinear scattering in the laser pulse with a duration of 20 fs, and their numerical results agree well with the analytical studies in the plane wave case. The foregoing work focuses on the scattering in continuous plane waves or multi-cycle laser pulses. Following successful research on laser pulse technology, ultrashort laser pulses with durations less than 5 fs are now available as research tools now. In this case, the laser pulse contains about one or two optical cycles, the laser intensity varies almost as rapidly as the laser oscillations and the time variation of the electric field depends sensitively on the initial phase of the few-cycle laser pulse. Due to these properties of few-cycle pulses, many novel and attractive phenomena in laser–atom interactions, such as photoionization and high harmonics generation, have been demonstrated theoretically and observed experimentally in the few-cycle regime. However, most of the studies focused mainly on nonlinear scattering with a laser pulse with a duration of more than 20 fs. Theoretical and experimental research on laser electron radiation with few-cycle pulses has been limited and the full spatial characteristics of the radiation in the cases of circularly polarized few-cycle laser pulse did not receive attention in earlier studies.

In the present paper, the previous investigations of radiation from electron oscillations driven by laser pulses to the few-cycle regime have been investigated. The emission generated from electron oscillations driven by a circularly polarized few-cycle

laser pulse of different intensity shows many different characteristics in contrast to the plane wave and multi-cycle pulse cases. For all initial phases, the well-known fourfold symmetry of the radiation angular distribution is broken in the few-cycle regime. These phenomena are illustrated from the point of view of electron relativistic dynamics and properties of the few-cycle pulse.

2 Interaction Model and Formulation

For a Gaussian laser pulse, the vector potential can be expressed as:

$$a(\eta) = a_0 \exp(-\eta^2 / 2L^2)[\cos(\eta + \phi_0)\hat{x} + \delta \sin(\eta + \phi_0)\hat{y}] \quad \ldots(1)$$

where a_0 is the peak amplitude normalized by mc^2 / e, $\eta = z - t$, $L = d / 2$ and d the laser pulse width, δ the polarization parameter for circular polarization $\delta = \pm 1$. φ_0 is the initial phase of the laser pulse. φ_0 is different from the initial phase that electron experiences when it enters the field. In the above definitions, space and time coordinates are normalized by k_0^{-1} and ω_0^{-1}, respectively, and ω_0 and k_0 are the laser frequency and wave number, respectively. m and e are the electron mass and charge, respectively.

The schematic geometry of laser-electron interaction is shown in Fig. 1. It is assumed that the laser pulse propagates along the $+\hat{\mathbf{z}}$ axis and an electron is initially stationary at the origin of the coordinate axes. The radiation direction is $\mathbf{n} = \sin\theta\cos\phi\hat{\mathbf{x}} + \sin\theta\sin\phi\hat{\mathbf{y}} + \cos\theta\hat{\mathbf{z}}$ (Fig. 1). In this expressions, θ and ϕ have the usual meanings as per the spherical coordinate system with the $\hat{\mathbf{z}}$ axis aligned along the electron longitudinal motion.

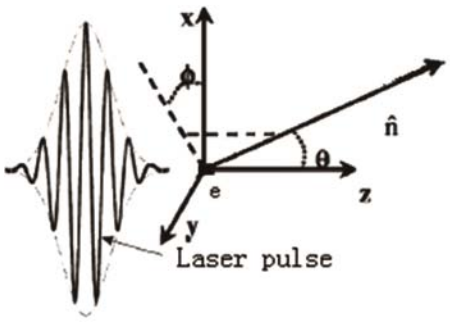

Fig. 1 — Schematic diagram showing the interaction of an incident intense circularly polarized few-cycle laser pulse with a stationary electron, we assume the laser field propagation along +*z* axis

The motion of an electron in an electromagnetic wave is described by the Lorentz equation[7,8,13] :

$$d_t(\mathbf{p} - \mathbf{a}) = -\nabla_a(\mathbf{a} \cdot \mathbf{u}) \quad \ldots(2)$$

together with an energy equation

$$d_t \gamma = \mathbf{u} \cdot \partial_t \mathbf{a} \quad \ldots(3)$$

where $\mathbf{u}$ is the velocity of an electron normalized by c, $\mathbf{p} = \gamma\mathbf{u}$ is the normalized momentum, $\gamma = (1 - u^2)^{-1/2}$ is the relativistic factor or normalized energy, and the ∇_a in Eq. (2) acts on $\mathbf{a}$ only. Note that Eqs. (2) and (3) are the exact one.

As the solution of 1D wave equation, the normalized vector potential $\mathbf{a} = \mathbf{a}(\eta)$. The quantities describing electron motion are assumed to be functions of η as well. With $\partial_z = \partial_\eta$ and $\partial_t = -\partial_\eta$, one gets from Eqs (2) and (3).

$$\gamma\mathbf{u}_\perp = \mathbf{a}, \ \gamma(u_z - 1) = \varepsilon \quad \ldots(4)$$

$$\gamma = -(1 + a^2 + \varepsilon^2)/2\varepsilon \quad \ldots(5)$$

In Eqs 4 and 5, we have assumed the transverse velocity $\mathbf{u}_\perp = 0$ when $\mathbf{a} = 0$, ε is a constant of the motion to be determined by the initial conditions on the electron motion. The motion of the electron can be fully determined; the velocity and displacement can be expressed as functions of η:

$$\mathbf{u}_\perp = \mathbf{a} / \gamma, \ u_z = 1 + \varepsilon / \gamma \quad \ldots(6)$$

$$r_\perp = \frac{1}{\varepsilon}\int \mathbf{a} d\eta, \ r_z = \frac{1}{2\varepsilon^2}\int (\varepsilon^2 - 1 - a^2) d\eta \quad \ldots(7)$$

where $r_\perp$ and r_z are the transverse and longitudinal displacement of the electron, respectively.

Electron in relativistic motion emits radiation, the radiated power per unit solid angle is given[8,12,17] by :

$$\frac{dP(t)}{d\Omega} = \left[\frac{\left|\mathbf{n} \times [(\mathbf{n} - \mathbf{u}) \times d_t \mathbf{u}]\right|^2}{(1 - \mathbf{n} \cdot \mathbf{u})^6}\right]_{t'} \quad \ldots(8)$$

where the radiation power is normalized by $e^2\omega_0^2/4\pi c$ and t' is the electron's time or retard time. The relation between t' and t is given by:

$$t = t' + R\,,\; R \sim R_0 - \mathbf{n}\cdot\mathbf{r} \qquad \ldots(9)$$

where R_0 is the distance from the origin to the observer and $\mathbf{r}$ is the position vector of the electron. Here the observation point is assumed to be far away from the region of space where electron acceleration occurs.

3 Results and Discussion

We begin by looking at the motion of the electron from the point at which it is overtaken by the front of the circularly polarized few-cycle laser pulse until it is left behind the trailing edge of the pulse, i.e. from the point of entrance till the point of the exit from the region of interaction with the laser pulse, respectively. By solving Eqs (6) and (7), we can obtain the electron trajectory, velocity and acceleration during the interaction.

The electron trajectories of an electron observed from the laboratory frame during the intense circularly polarized few-cycle laser pulse for different initial phase $\varphi_0 = 0$ (black line), $\varphi_0 = \pi/2$ (red line), $\varphi_0 = \pi$ (green line), and $\varphi_0 = 3\pi/2$ (blue line) are shown in Fig. 2. The electron's initial energy is $\gamma_0 = 1$, the peak amplitude of the laser pulse is $a_0 = 3.0$, the pulse duration is $\mathrm{d} = 1\lambda_0$ (3.3fs), and the wavelength of the laser pulse is $\lambda_0 = 1\mu m$. The normalized vector potential corresponds to an intensity of $I = 1.24\times10^{19} W/cm^2$. The laser pulse propagates along the $+\hat{\mathbf{z}}$ axis and the electron is at (0, 0, 0) initially, where the radial ponderomotive force is about zero. As shown in Fig. 2, the electron trajectories show different asymmetric spiral patterns for different initial phase which do not resemble with fourfold symmetric spiral patterns in the multi-cycle pulse field[8,11] and the quivering amplitude is modulated by the envelope of the driving laser pulse. The radial maximum displacement is about 0.5 λ_0 and the electron drift is about $4\lambda_0$ along the $+\hat{\mathbf{z}}$ axis during the interaction. The quivering amplitude of an electron at a laser intensity of $10^{19} W/cm^2$ amounts to $0.5\mu m$ which is much smaller as compared to a typical beam size of $20\mu m$ in diameter in the real experiments. Hence, the relative variation of laser intensity during the quivering motion of an electron can be neglected. Thus, the Gaussian wave approximation in Eq. (1) is valid and adopted for this calculation. In Fig. 2, it can be seen that the electron never moves backward in the lab frame which was also demonstrated both experimentally[9,10] and theoretically[8,12,18] in the previous work.

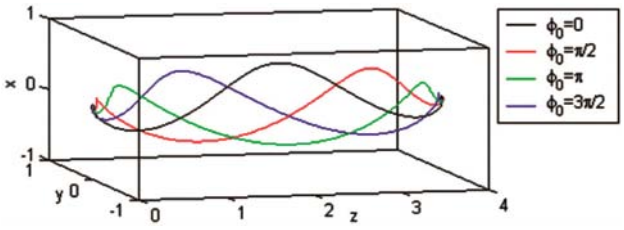

Fig. 2 — Trajectories of an electron during the intense circularly polarized few-cycle laser pulse for different initial phase φ_0=0 (black line), φ_0=π/2 (red line), φ_0=π (green line), and φ_0=3π/2 (blue line). The electron's initial energy is γ_0=1, the peak amplitude of the laser pulse is a_0=3.0, the pulse duration is d=1λ_0 (corresponding to 3.3 fs) , and the wavelength of the laser pulse is λ_0=1 μm

Now, we consider the full spatial characteristics of the electron's radiation power in the few-cycle regime. As we know, in the plane wave and multi-cycle circularly polarized laser pulse cases, the radiated power per unit solid angle is the same in all the directions for laser pulse with low power intensities and the radiation is directed toward the $+\hat{\mathbf{z}}$ axis (the polar angle $\theta < \pi/2$) with a narrower divergence and is tipped forward more and more with the increase of laser intensity. The azimuthal angular distribution is fourfold symmetric with respect to the electric and magnetic field directions[6,8,12]. Whereas in the few-cycle laser pulse, as shown in Fig. 2, the electron relativistic dynamics shows many novel characteristics, which will lead to significant influence on the radiation. The characteristics of full spatial distribution of electron emission during a circularly polarized few-cycle laser pulse with different intensity and different initial phases have been plotted in Fig. 3 ($a_0 = 0.01$), Fig. 4 ($a_0 = 0.1$), Fig. 5 ($a_0 = 0.5$), Fig. 6 ($a_0 = 1.0$), Fig. 7 ($a_0 = 1.5$), Fig. 8 ($a_0 = 2.0$), Fig. 9 ($a_0 = 2.5$), and Fig. 10 ($a_0 = 3.0$) and for different initial phase (a) $\varphi_0 = 0$, (b) $\varphi_0 = \pi/2$, (c) $\varphi_0 = \pi$ and (d) $\phi_0 = 3\pi/2$. Please note that the colour-coding for

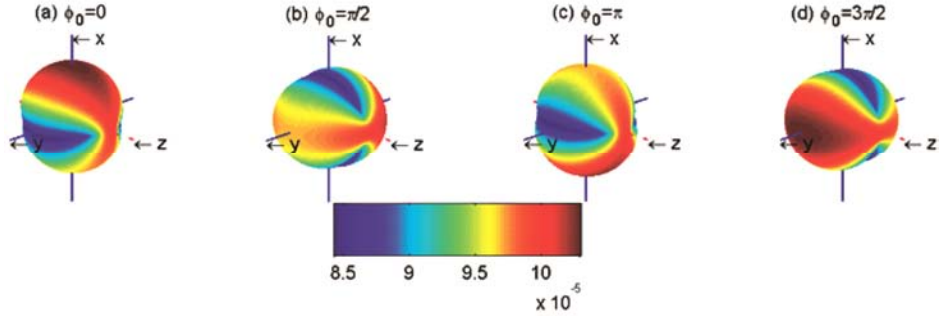

Fig. 3 — Full spatial distributions of the electron's radiation power during the intense circularly polarized few-cycle laser pulse of a_0=0.01 for different initial phase (a) φ_0=0, (b) φ_0=π/2, (c) φ_0=π and (d) φ_0=3π/2. All of the other calculation parameters are the same as those in Fig. 2

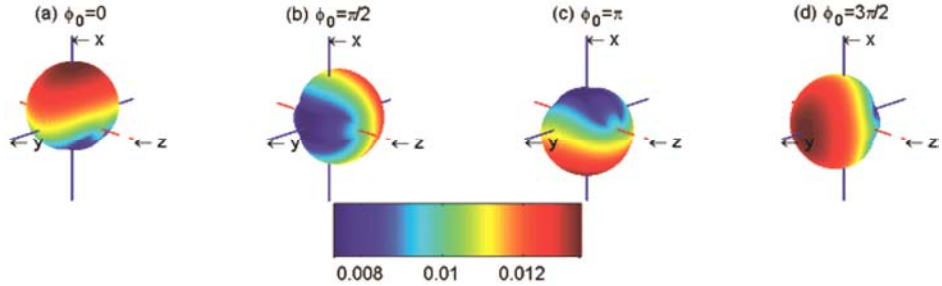

Fig. 4 — Full spatial distributions of the electron's radiation power during the intense circularly polarized few-cycle laser pulse of a_0=0.1 for different initial phase (a) φ_0=0, (b) φ_0=π/2, (c) φ_0=π and (d) φ_0=3π/2. All of the other calculation parameters are the same as those in Fig. 2

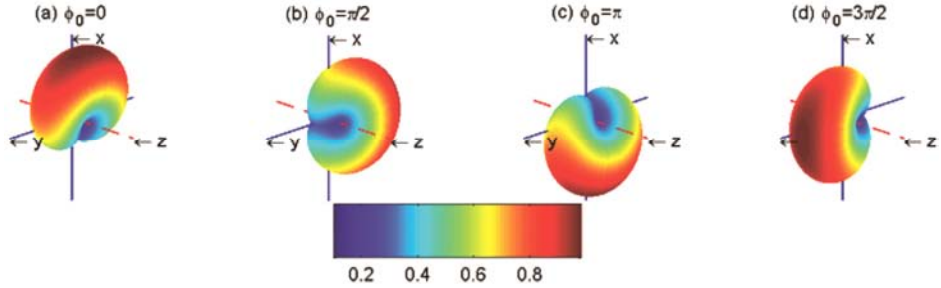

Fig. 5 — Full spatial distributions of the electron's radiation power during the intense circularly polarized few-cycle laser pulse of a_0=0.5 for different initial phase (a) φ_0=0, (b) φ_0=π/2, (c) φ_0=π and (d) φ_0=3π/2. All of the other calculation parameters are the same as those in Fig. 2

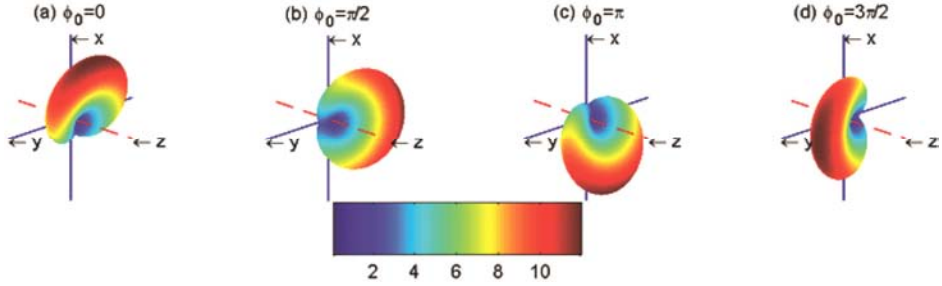

Fig. 6 — Full spatial distributions of the electron's radiation power during the intense circularly polarized few-cycle laser pulse of a_0=1.0 for different initial phase (a) φ_0=0, (b) φ_0=π/2, (c) φ_0=π and (d) φ_0=3π/2. All of the other calculation parameters are the same as those in Fig. 2

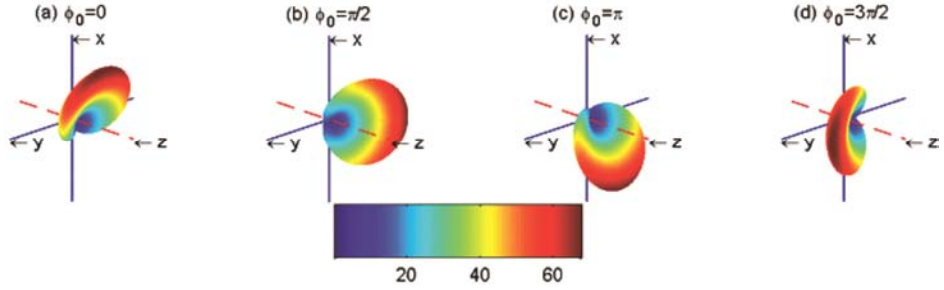

Fig. 7 — Full spatial distributions of the electron's radiation power during the intense circularly polarized few-cycle laser pulse of a_0=1.5 for different initial phase (a) φ_0=0, (b) $\varphi_0=\pi/2$, (c) $\varphi_0=\pi$ and (d) $\varphi_0=3\pi/2$. All of the other calculation parameters are the same as those in Fig. 2

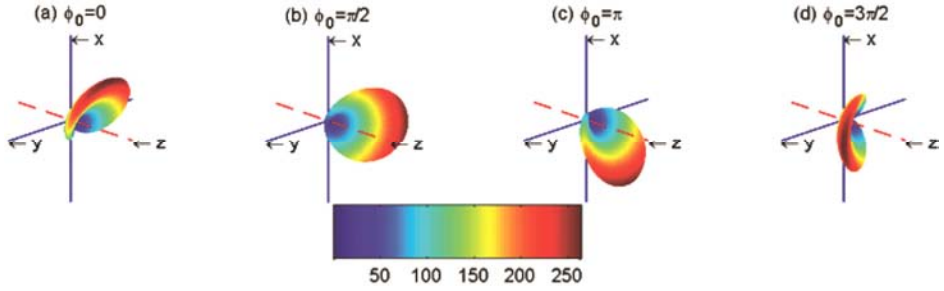

Fig. 8 — Full spatial distributions of the electron's radiation power during the intense circularly polarized few-cycle laser pulse of a_0=2.0 for different initial phase (a) φ_0=0, (b) $\varphi_0=\pi/2$, (c) $\varphi_0=\pi$ and (d) $\varphi_0=3\pi/2$. All of the other calculation parameters are the same as those in Fig. 2

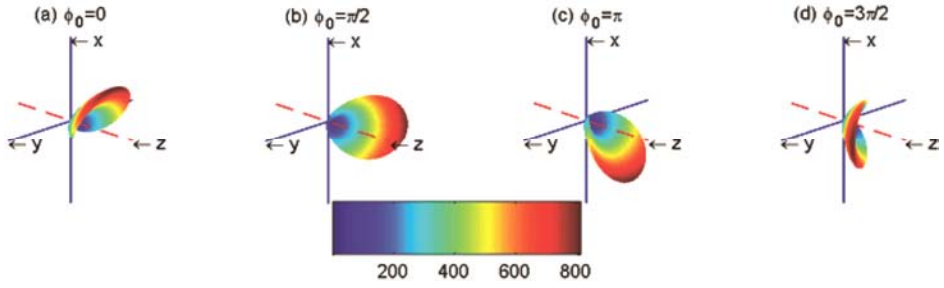

Fig. 9 — Full spatial distributions of the electron's radiation power during the intense circularly polarized few-cycle laser pulse of a_0=2.5 for different initial phase (a) φ_0=0, (b) $\varphi_0=\pi/2$, (c) $\varphi_0=\pi$ and (d) $\varphi_0=3\pi/2$. All of the other calculation parameters are the same as those in Fig. 2

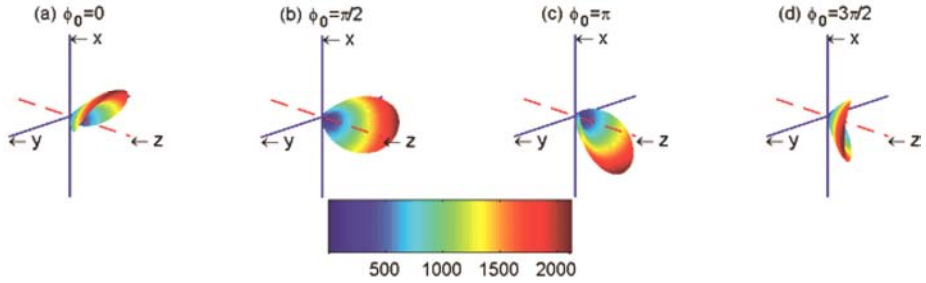

Fig. 10 — Full spatial distributions of the electron's radiation power during the intense circularly polarized few-cycle laser pulse of a_0=3.0 for different initial phase (a) φ_0=0, (b) $\varphi_0=\pi/2$, (c) $\varphi_0=\pi$ and (d) $\varphi_0=3\pi/2$. All of the other calculation parameters are the same as those in Fig. 2

these eight columns is different for different laser intensity. As shown in Figs (3-10), the results show emission process is highly sensitive to laser intensity and initial phases. The patterns of the full spatial distribution of electron emission are different for various intensity and the fourfold symmetry of the angular distribution is broken.

First we focus on the influence of laser intensity on the full spatial distribution. One can clearly see from Fig. 3, that the radiated power per unit solid angle is like a symmetrical smiling face for laser pulse with lower power intensities (a_0=0.01). In fact, the emission is approximately the same in all the directions (spherically symmetric shape radiation). The minimum and the maximum of the radiations are 0.000084285 and 0.0001034, respectively. For $a_0 = 0.1$ (Fig. 4), the radiation looks like a red goldfish shape. The radiation pattern shown in Figs 5 and 6 have a embryo like shape. The radiation pattern shown in Figs 7 and 8 looks like a shell. Figs 9 and 10 have a cat's ear like shape. The radiation is directed towards the $+\hat{\mathbf{z}}$ axis with a narrower divergence and gets more and more pointed forward with the increase of laser intensity. We define the angle θ_M at which the radiation becomes maximum. $\theta_M = 90^\circ$ for $a_0 = 0.01$ [Fig. 3], $\theta_M = 87^\circ$ for $a_0 = 0.1$ [Fig. 4], $\theta_M = 76^\circ$ for $a_0 = 0.5$ [Fig. 5], $\theta_M = 63^\circ$ for $a_0 = 1.0$ [Fig. 6], $\theta_M = 53^\circ$ for $a_0 = 1.5$ [Fig. 7], $\theta_M = 45^\circ$ for $a_0 = 2.0$ [Fig. 8], $\theta_M = 39^\circ$ for $a_0 = 2.5$ [Fig. 9] and $\theta_M = 34^\circ$ for $a_0 = 3.0$ [Fig. 10]. Thus, the angle θ_M can be used as a parameter to measure the intensity of circularly polarized laser pulses in the experiments.

Now, we examine the influence of initial phase on the full spatial distribution taking laser intensity $a_0 = 3.0$ as an illustration. As shown in Fig. 10, at (a) $\varphi_0 = 0$, (b) $\varphi_0 = \pi/2$, (c) $\varphi_0 = \pi$, and (d) $\varphi_0 = 3\pi/2$, the patterns of the full spatial distribution of electron emission are of the same shape resembling a cat's ear and the fourfold symmetry of the angular distribution is broken. In detail, with $\varphi_0 = 0$, the radiation to the direction of the polar angle $\theta = 34^\circ$ and the azimuthal angle $\phi = 0^\circ$ is dominant, with $\varphi_0 = \pi/2$, the radiation to the direction of the polar angle $\theta = 34^\circ$ and the azimuthal angle $\phi = 90^\circ (\pi/2)$ is dominant. With $\varphi_0 = \pi$, the radiation to the direction of the polar angle $\theta = 34^\circ$ and the azimuthal angle $\phi = 180^\circ (\pi)$ is dominant and with $\varphi_0 = 3\pi/2$, the radiation to the direction of the polar angle $\theta = 34^\circ$ and the azimuthal angle $\phi = 270^\circ (3\pi/2)$ is dominant. It is a very interesting phenomenon that the azimuthal angle $\phi_{\max}$ of the maximal radiation is equal to the initial phase φ_0 of the few-cycle laser pulse, i.e., $\phi_{\max} = \varphi_0$. This phenomenon is primarily governed by the electron dynamics and properties of the circularly polarized few-cycle laser pulse that can be effectively used to measure the azimuthal angle $\phi_{\max}$ of the maximal radiation to obtain the initial phase of intense circularly polarized few-cycle laser pulses in experiments.

Figure 11 shows the dependence of the angle θ_M at which the radiation becomes maximum (solid curve) and the highest power per unit solid angle $(dP/d\Omega)_{max}$ (dashed curve) on the laser pulse intensities. The other laser parameters in this calculation are the same as those shown in Fig. 2. We find the angle θ_M decreases and the highest power per unit solid angle $(dP/d\Omega)_{max}$ increases with increasing the intensity of the laser pulse. The increase of a laser intensity enhances not only a total radiated power but also the radiation flux. This

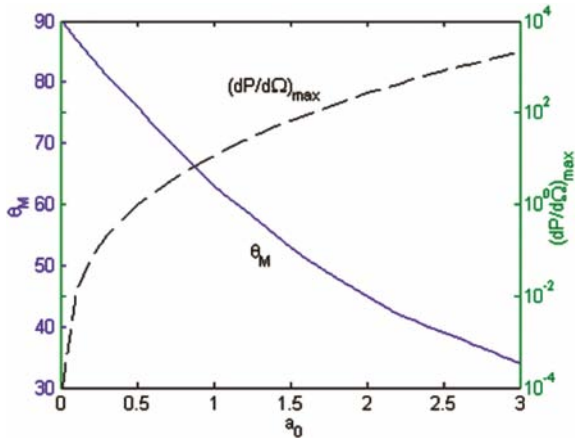

Fig. 11 — Dependence of the angle θ_M at which the radiation becomes maxim um (solid curve) and the highest power per unit solid angle $(dP/d\Omega)_{max}$ (dashed curve) on the laser pulse intensities. The other parameters are the same as in Fig. 2

characteristic makes the emitted radiation as a viable source to determine and measure the laser intensity. Well-defined radiation pattern has been proven to be useful source for many applications.

4 Conclusions

In conclusion, the dynamics and radiation characteristics of an electron in a circularly polarized few-cycle laser pulse are investigated theoretically and numerically in the cases of different initial phases. The results show that the electron motion depends sensitively on the initial phase of the driving laser pulse, which results in many remarkable initial phase-sensitive full spatial characteristics of the radiation. The emission generated from electron oscillations driven by a circularly polarized few-cycle laser pulse of different intensity shows many different characteristics in contrast to the plane wave and multi-cycle pulse cases. These phenomena are primarily governed by the electron dynamics and properties of the circularly polarized few-cycle laser pulse that can be effectively used to measure the initial phase of intense circularly polarized few-cycle laser pulse in experiments.

The vector potential in this paper models a laser pulse only approximately. A final note is in order concerning the possibility of observing the radiation predicted in this paper. This would involve employing an assembly of electrons and not just a single electron; that is, multi-electrons at different positions emitting radiations with time interval in electrons' frame of reference. The phase matching and perhaps other subtle issues of the radiations from different electrons may potentially make it quite difficult to observe such emitted radiation.

Acknowledgement

This work has been supported by the National Natural Sciences Foundation of China under Grant No. 10947170/A05 and No. 11104291, Natural science fund for colleges and universities in Jiangsu Province under Grant No. 10KJB140006, Natural Sciences Foundation of Shanghai under Grant No. 11ZR1441300 and Foundation of NJUPT under Grant No. NY212080 and sponsored by Jiangsu Qing Lan Project and STITP Project under Grant No. XZD2013003.

References

1 Zeitoun Ph, Faivre G & Sebban S, *Nature*, 431 (2004) 426.
2 Sprangle P, Ting A, Esarey E & Fisher A, *J Appl Phys*, 72 (1992) 5032.
3 Esarey E, Ride S K & Sprangle P, *Phys Rev E*, 48 (1993) 3003.
4 Yu Wei, Yu M Y, Ma J X & Xu Z, *Phys Plasmas*, 5 (1998) 406.
5 He F, Lau Y Y, Umstadter D P & Kowalczyk R, *Phys Rev Lett*, 90 (2003) 055002.
6 Lee K, Cha Y H, Shin M S, Kim B H & Kim D, *Phys Rev E*, 67 (2003) 026502.
7 Yu W, Li B W, Yu M Y, He F, Ishiguro S & Horiuchi R, *Phys Plasmas*, 12 (2005) 103101.
8 Youwei Tian, Yunqing Lu, Ying Zheng & Jianping Yang, *Optik*, 122 (2011) 1373.
9 Pogorelsky I V, Ben-Zvi I & Hirose T, *Phys Rev ST Accel Beams*, 3 (2000) 090702.
10 Rousse A, Phuoc K, Shah R, Pukhov A, Lefebvre E, Malka V, Kiselev S, Burgy F, Rousseau J-P, Umstadter D & Hulin D, *Phys Rev Lett*, 93 (2004) 135005.
11 Sarachik E S & Schappert G T, *Phys Rev D*, 1 (1970) 2738.
12 Jackson J D, *Classical Electrodynamics* (Wiley, New York, 1975).
13 Gibbon P, *IEEE J Quantum Electron*, 33 (1997) 1915.
14 Brau C A, *Phys Rev ST Accel Beam*, 7 (2004) 020701.
15 Krafft G A, *Phys Rev Lett*, 92 (2004) 204802.
16 Mourou G A , Tajima T & Bulanov S V, *Rev Mod Phys*, 78 (2006) 309.
17 Tian Youwei, Yu Wei, Xu Han, Wang Xin, Deng Degang & Senechad Vinod, *Optik*, 121 (2010) 808.
18 Gao Ju, *Phys Rev Lett*, 93 (2004) 2430011.